Model evaluation for glycolytic oscillations in yeast biotransformations of xenobiotics

L. Brusch [a,b,*,1], G. Cuniberti [c,b,2], M. Bertau [d]

[a] *Centre de Bioingénierie Gilbert Durand INSA-DGBA, Av. de Rangueil 135, F-31077 Toulouse Cedex 4, France*

[b] *Max-Planck-Institut für Physik komplexer Systeme, Nöthnitzer Straße 38, D-01187 Dresden, Germany*

[c] *Institute for Theoretical Physics, University of Regensburg, D-93040 Regensburg, Germany*

[d] *Institut für Biochemie, Technische Universität Dresden, D-01062 Dresden, Germany*

Abstract

Anaerobic glycolysis in yeast perturbed by the reduction of xenobiotic ketones is studied numerically in two models which possess the same topology but different levels of complexity. By comparing both models' predictions for concentrations and fluxes as well as steady or oscillatory temporal behavior we answer the question what phenomena require what kind of minimum model abstraction. While mean concentrations and fluxes are predicted in agreement by both models we observe different domains of oscillatory behavior in parameter space. Generic properties of the glycolytic response to ketones are discussed.

1 Introduction

The reductionist attempt to identify the function of all genetic constituents of a living organism is one of the major goals of the post-genomic research [1,2]. In a living cell, however, single molecular constituents are linked together in a *complex network* including gene regulation, signaling and metabolic pathways [3,4]. Whether the detailed knowledge of the individual properties of

* Corresponding author.
Email address: brusch@mpipks-dresden.mpg.de (L. Brusch).

[1] LB is supported by the Max Planck Society through an Otto Hahn fellowship.
[2] GC research is funded by the Volkswagen Foundation.

metabolites taking part in enzymatic reactions may help to infer the large scale behavior of the living cell is another question challenging life-scientists, and its answer will necessarily imply a highly inter-disciplinary cooperative effort.

A recent study of gene regulatory networks for early fruit fly development has suggested that the inherited robustness of the network's behavior may solely result from the network's topology [5]. This robustness may render the observed behavior insensitive to the quantitative details of the microscopic interactions. Hence modeling of such networks was successful even for rather crude approximations of the details. Other findings on artificial gene circuits showed a broad variety of different functions despite the same topology, suggesting that quantitative details become important for some topologies [6]. Moreover, the construction of a mathematical model and the corresponding abstraction of the complex intracellular network are always confronted with the problem of neglecting "unnecessary" details. The issue of the appropriate level of abstraction has been disputed particularly in the case of metabolic networks. Therein it has been suggested that modeling efforts risk to be no longer taken serious by experimentalists if modeling is continued by means of "too" strong abstractions or falsified toy models [7].

Here we compare predictions from two models of different levels of abstraction to characterize the consequences of neglecting details. For this fundamental study we choose the metabolic network of glycolysis (Fig. 1) in baker's yeast (*Saccharomyces cerevisiæ*) which is of particular interest to biotechnology [8,9] and models of different degree of complexity have been suggested and used [10,11,12,13,14,15,16]. We choose two models that translate the metabolic network into systems of ordinary differential equations (ODEs), a procedure that is well established [17,18,19]. Our subsequent analysis treats the ODEs fully nonlinear and focuses on the temporally asymptotic, self-organising behavior of the models. The distinction between steady and oscillatory states in the models appears to be crucial, since several physiological advantages of the latter have been proposed. The dependences of the concentrations and fluxes on external control parameters are numerically computed via a bifurcation analysis [20,21]. This approach enables detailed studies of large parameter spaces that would be more time consuming by simulation of the complete time courses including transient dynamics [22]. This issue will gain importance as the analysed theoretical models increase in size and complexity.

In order to test the predictive power of both models, we perturb both models by the same set of simple equations that account for the conversion of a xenobiotic (here we choose a ketone) by a single enzyme (here alcohol dehydrogenase) into a chiral carbinol which consumes the cofactor nicotinamide adenine dinucleotide (NADH), see Fig. 1(a). This particular perturbation was chosen both for its pharmaceutical relevance and its broad impact on the back-

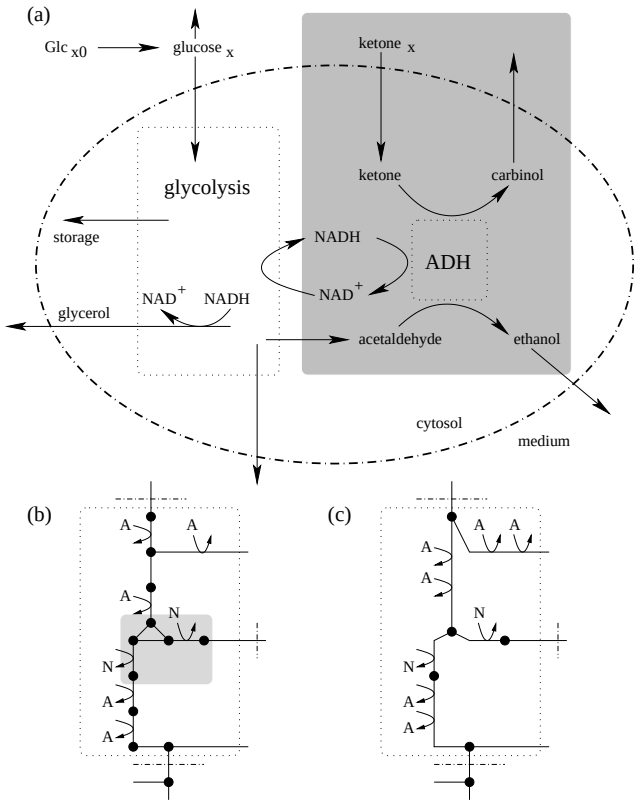

Fig. 1. Schematic view of a yeast cell in chemostat culture and models of different degree of abstraction. (a) Glucose influx at constant flow rate is parameterized by the concentration $[\mathrm{Glc}_x]_0$. The perturbation (dark shaded box) is controlled by the concentration $[\mathrm{K}_x]$ of ketone in the medium and described by the same set of equations with identical parameter values for two models. The full scale model (b) and core model (c) describe glycolysis (dotted box) at different degrees of complexity. Dots (lines) denote metabolites (reactions), "N" ("A") stands for NADH (ATP) and the light shaded box in (b) is considered in detail in Subsec. 3.2.

bone of glycolysis via the NADH mediated interference with the redox balance of the cell. The pharmaceutical interest stems from the increasing demand for stereoisomerically pure pharmacologically active compounds (PACs). The stereo-geometry of PACs essentially determines the physiological effects of a chiral drug, as the thalidomide (contergan®) tragic showed in the 1950s [23]. Stereoisomerically pure carbinols are central precursors of modern, innovative pharmaceuticals and make for more than 50% of all essential substructures in pharmaceuticals [9]. Today stereo-selective carbinol synthesis by means of biotransformation, *i.e.* chemical reactions catalyzed by enzymes *in vivo*, is indispensable for the production of PACs [24,25,26]. Further progress in the understanding and rational manipulation of biotransformatory carbinol syntheses strongly depends on mathematical models that account for the limiting reproduction of the cofactor (NADH in the considered case) and the underlying regulatory networks [27,28]. The models studied in this paper also constitute a first step in this direction. In the future we will extend the analysis to

other eucaryote's metabolic responses to a range of pharmacologically active compounds.

We emphasize the exposure of systems in oscillatory states to xenobiotics as a sensitive experimental probe of the network's global response. The global response is experimentally accessible via NADH-fluorescence, and oscillatory or steady behavior is easily distinguishable as individual cells synchronize their oscillations [11]. The temporal frequency of the oscillations can be measured with high accuracy.

The paper is organized as follows. In Sec. 2 two models of glycolysis and the unique set of equations representing the perturbation are introduced and the employed numerical method of bifurcation analysis is outlined. Section 3 presents our results which are discussed in Sec. 4.

2 Models and Methods

The glycolytic pathway of *Saccharomyces cerevisiæ* fermenting glucose to ethanol is one of the best studied metabolisms from both the experimental and modeling side [10,11,12,13,14,15,16]. We consider two different mathematical models in terms of ODEs that identically represent the topology of the glycolytic pathway under anaerobic conditions, see Fig. 1(b),(c).

2.1 Glycolysis

Specifically we start from the full scale model of glycolysis devised by Hynne *et al.* [15] and compare its predictions with those of a core model with the same topology adapted from Wolf *et al.* [12]. Public domain "Silicon Cell" versions of the models can be found at `http://www.jjj.bio.vu.nl`, including a graphical overview and the mathematical expressions. The full scale model contains 22 variables for concentrations of involved metabolites and quantitatively accounts for most known details on enzyme regulation in order to precisely describe the supercritical onset of oscillations as observed experimentally [11,15]. The core model has been derived from the original 9 variable model [12] by addition of the variable S_1^{ex} (extracellular glucose) and the corresponding flux balance of the medium $j_0^{ex} = y_{\mathrm{vol}} k([\mathrm{Glc}_x]_0 - S_1^{ex})$ and a simple form of glucose transporter saturation $j_0 = k_0(S_1^{ex} - S_1)/(S_1^{ex} - S_1 + K_{\mathrm{trans}})$ as well as lactonitrile formation $j_{7\mathrm{CN}} = y_{\mathrm{vol}} k_{\mathrm{CN}} S_4^{ex}$ in the presence of cyanide. A storage flux $j_{\mathrm{Store}} = k_{\mathrm{Store}} S_1 A_3$ is included in analogy with the full scale model but as a consequence of combining the three reactions downstream of glucose, j_{Store} is fed by intracellular glucose S_1 in the core model instead of glucose-6-

parameter	value in present model	value in model of Ref. [12]
$y_{\mathrm{vol}} \cdot k$ (min^{-1})	$59 \cdot 0.048$	1.3
k_1 (mM^{-1} min^{-1})	6211.86	100.0
k_2 (mM^{-1} min^{-1})	38.3756	6.0
k_3 (mM^{-1} min^{-1})	126819	16.0
k_5 (min^{-1})	22.2857	1.28
k_6 (mM^{-1} min^{-1})	6.93908	12.0
κ (min^{-1})	24.7	13.0
q	4.0	4.0
K_I (mM)	0.52	0.52
N_{total} (mM)	0.98	1.0
A_{total} (mM)	3.6	4.0
k_0 (mM min^{-1})	48.1	-
K_{trans} (mM)	0.002	-
k_{Store} (mM^{-1} min^{-1})	17.1	-
k_{CN} (min^{-1})	0.01477	-
ADH_{total} (mM)	0.01	-
k_1^{ADH} (mM^{-2} min^{-1})	80800	-
k_2^{ADH} (min^{-1})	1000	-
k_3^{ADH} (min^{-1})	5400	-

Table 1
Comparison of parameters for our core model with the original model (Reference) by Wolf *et al.* [12]. The values of $y_{\mathrm{vol}}, k, \kappa, N_{\mathrm{total}}, A_{\mathrm{total}}, ADH_{\mathrm{total}}, k_{1\ldots3}^{\mathrm{ADH}}$ are identical in both models and taken (except for ADH_{total} and $k_{1\ldots3}^{\mathrm{ADH}}$) from Ref. [15]. For the full scale model, parameters are identical with Hynne *et al.* [15].

phosphate in the full scale model. The consumption of two subsequent entities ATP per glucose for storage would contribute with $-2j_{\mathrm{Store}} = -2k_{\mathrm{Store}}S_1A_3$ to the ATP balance. However, we find that this term overestimates the feedback of a varying glucose concentration on the ATP balance and we always observed subcritical onsets of oscillations under this assumption. Indeed, not intracellular glucose but glucose-6-phosphate is the substrate and allosteric activator of the pathway to carbohydrate storage [29]. In the ATP balance, we therefore keep the ATP consumption for storage included in the term $-k_5A_3$ of unspecific ATP consumption in line with the original 9 variable model [12]. The remaining nomenclature and kinetic terms are identical with Ref. [12] but we have fitted a new set of parameters (see Table 1) to describe the same data as the full scale model.

In both models, we have replaced the reduction of acetaldehyde (ACA) to ethanol (EtOH) by the same simple reaction scheme:

$$\begin{aligned} &\mathrm{ACA} + \mathrm{NADH} + \mathrm{ADH} \quad \underset{k_2^{\mathrm{ADH}}}{\overset{k_1^{\mathrm{ADH}}}{\rightleftharpoons}} \\ &\mathrm{ADH}_{\mathrm{ACA}} \quad \overset{k_3^{\mathrm{ADH}}}{\rightarrow} \quad \mathrm{ADH} + \mathrm{NAD}^+ + \mathrm{EtOH} \end{aligned} \tag{1}$$

which later enables the coupling with a second reaction that utilizes the same enzyme alcohol dehydrogenase (ADH; EC 1.1.1.1). We introduce the concentration $[\mathrm{ADH_{ACA}}]$ of the bound enzyme as an additional variable with the ODE

$$\frac{\mathrm{d}[\mathrm{ADH_{ACA}}]}{\mathrm{dt}} = v^{+}_{\mathrm{ADH,ACA}} - v^{-}_{\mathrm{ADH,ACA}} \ . \tag{2}$$

Its gain ($v^{+}_{\mathrm{ADH,ACA}}$) and loss ($v^{-}_{\mathrm{ADH,ACA}}$) fluxes are described by simple mass action kinetics in agreement with the Michaelis-Menten term used for the complete reaction in the original full scale model [15].

$$v^{+}_{\mathrm{ADH,ACA}} = k_1^{\mathrm{ADH}} \cdot [\mathrm{ACA}] \cdot [\mathrm{NADH}] \cdot [\mathrm{ADH}] \tag{3}$$

$$v^{-}_{\mathrm{ADH,ACA}} = k_2^{\mathrm{ADH}} \cdot [\mathrm{ADH_{ACA}}] + k_3^{\mathrm{ADH}} \cdot [\mathrm{ADH_{ACA}}] \tag{4}$$

The unbound form of the enzyme is computed from the total amount ADH_{total} of the enzyme by

$$[\mathrm{ADH}] = ADH_{\mathrm{total}} - [\mathrm{ADH_{ACA}}] \tag{5}$$

whereas the concentration of $\mathrm{NAD^+}$ follows from

$$[\mathrm{NAD^+}] = N_{\mathrm{total}} - [\mathrm{NADH}] - [\mathrm{ADH_{ACA}}] \ . \tag{6}$$

The ODEs for [NADH], [ACA] and [EtOH] have also been updated by the new expressions for the fluxes. We have fixed two of the four new parameters to $ADH_{\mathrm{total}} = 10\mu\mathrm{M}$ and $k_2^{\mathrm{ADH}} = 1000\ \mathrm{min}^{-1}$ and computed the remaining two self-consistently from the fluxes in the original full scale model [15], for all values see Table 1. This procedure preserved the full scale model's behavior as verified in Table 2 and by comparison of the bifurcation diagrams Fig.2 (a) and Fig. 5 in Ref. [15]. Identical equations (2)-(6) and the same parameter values are used in both models.

Although the core model possesses the same topology as the full scale model, it uses simple mass action kinetics for all lumped steps of the pathway [12]. One single regulatory interaction has been included, specifically the regulation of 6-phosphofructokinase (PFK; EC 2.7.1.11) via ATP. This strong abstraction of the core model is sufficient to reproduce glycolytic oscillations [12].

We calculated a new set of parameters (see Table 1) for the core model such that the onset of oscillations at $[\mathrm{Glc}_x]_0$=18.5 mM is captured to the same accuracy (see Table 2) as in the full scale model, which had particularly been optimized to describe the onset of oscillations. To fit the core model, we inserted the known values of fluxes and concentrations from the full scale model

Variable in core	and full scale model	Core model	Full scale model	Reference
$[\mathrm{Glc}_x]_0$	$[\mathrm{Glc}_x]_0$	18.5	18.501	18.5
S_1^{ex}	$[\mathrm{Glc}_x]$	1.54982	1.55409	1.55307
S_1	[Glc]	0.560999	0.573935	0.573074
S_2	[DHAP]	2.08167	2.97161	2.95
S_3	[BPG]	0.000266672	0.00026973	0.00027
S_4	[ACA]	1.48032	1.49748	1.48153
S_4^{ex}	$[\mathrm{ACA}_x]$	1.28731	1.30226	1.28836
N_2	[NADH]	0.330046	0.329872	0.33
A_3	[ATP]	2.08505	2.09875	2.1
j_{in}	j_{in}	48.0	47.99	48.0
j_{storage}	j_{storage}	20.0	19.90	20.0
j_{Glyc}	j_{Glyc}	4.77	4.82	4.8
j_{EtOH}	j_{EtOH}	46.46	46.54	46.4
j_{outACA}	j_{outACA}	4.77	4.82	4.8

Table 2
Comparison of metabolite concentrations (top, all values are in mM and accurate to six significant digits) and fluxes (bottom, rounded and in mM min^{-1}) for both models at the onset of oscillations. Reference values are taken from a comprehensive modeling effort that incorporated available experimental data (Table 6 in [15]) and only a subset of the full scale model's variables are shown. All others match the Reference equally well.

(Table 6 in Ref. [15], here included as Reference in Table 2) into the expressions of the core model and calculated those parameters k_i which are factors of mass action terms. This strategy was partly used in Ref. [15]. Parameters k_i of flux terms that involve a yet undetermined saturation constant were expressed as functions (with inserted values of fluxes and concentrations at onset) of the respective saturation constant. Then a steady state at the onset of oscillations (Hopf bifurcation) was determined for an initial choice of the unknown parameters and numerically continued along curves in the space of unknown parameters (see Methods below). Note, this strategy is very efficient since each run explores two unknown parameters simultaneously which are linked by the constraint of reproducing a Hopf bifurcation. We monitored the values of the resulting fluxes and fixed that combination of remaining parameters with closest correspondence of the computed fluxes to the data from the full scale model (Tables 7,8 in Ref. [15]). The computed concentrations at the onset of oscillations in the core model were also in good agreement with those of the full scale model (see Table 2). The temporal period of the oscillations near onset was close to 0.65 min in the full scale model and 0.25 min in the core model.

Fig. 2 shows that the new set of parameters also yields a supercritical onset of the oscillations in the core model in agreement with the full scale model and experiments [11,15]. This set of parameters is therefore well suited for further studies of synchronisation phenomena in a multicellular context [13]. Note, that both models also share a second oscillatory domain at lower glucose con-

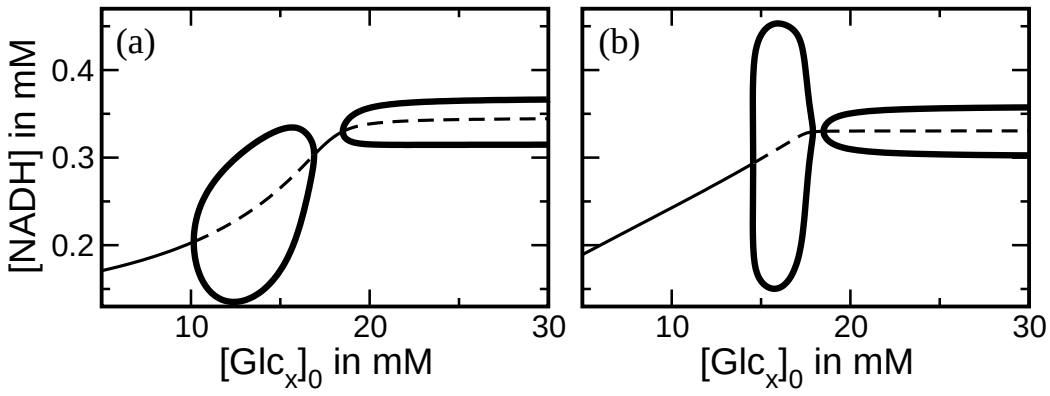

Fig. 2. Bifurcation diagrams of (a) the full scale model and (b) the core model of glycolysis showing steady states (thin curves) as well as minimum and maximum (thick) of NADH oscillations for varied inflow glucose concentration $[\mathrm{Glc}_x]_0$. Solid (dashed) curves represent stable (unstable) states.

centration. This has also been observed in the original full scale model (Fig. 8 in Ref. [15]) but so far not in experiments. This agreement of both models' predictions may stem from their identical topology but still is remarkable since it covers a parameter range outside of that where the models had been fitted.

Altogether, both the full scale model and the core model show very similar behavior and create the impression that quantitative details are largely irrelevant when the model is analysed in the same context that had already been used to determine the remaining unknown parameters. Hence "predictions" from a simplified model are reliable for conditions similar to those considered in the model's construction, *e.g.* both models predict a second oscillatory domain for low glucose supply. However, we want to test the reliability of the core model under conditions that may be very different from those included during parameter optimization. Such reliability is essential for the rational improvement of biotechnological processes beyond the conditions applied so far.

2.2 Perturbation of the redox-balance

Both the full scale model and the core model have been augmented with the same set of equations that account for the biotransformation of a xenobiotic ketone. In the considered case the ketone ethyl acetoacetate is reduced by alcohol dehydrogenase (ADH; EC 1.1.1.1) to enantiomerically pure ethyl *L*-3-hydroxybutyrate (carbinol). Although this reaction has been studied extensively, little is known about how the intracellular enzymes interact [30,31,32,33,34,35]. Currently, two enzymes, *D*-directing β-ketoacyl reductase (KAR; EC 1.1.1.100) and *L*-directing ADH are known to be involved in the asymmetric reduction of the substrate [28,36]. Yet, KAR activity is negli-

gible with a large excess of sugar present. Hence, the overall stereo-selectivity of the bioconversion largely depends on cell physiology [28].

In analogy to the reduction of acetaldehyde (ACA) in reaction (1), we now consider the reduction of ketone (K) to carbinol (C) by the same simple reaction scheme:

$$\begin{array}{lll} \mathrm{K} + \mathrm{NADH} + \mathrm{ADH} & \overset{k_4^{\mathrm{ADH}}}{\underset{k_5^{\mathrm{ADH}}}{\rightleftharpoons}} & \\ \mathrm{ADH_K} & \overset{k_6^{\mathrm{ADH}}}{\rightarrow} & \mathrm{ADH} + \mathrm{NAD^+} + \mathrm{C} \end{array} \tag{7}$$

with rate constants $k_4^{\mathrm{ADH}}, k_5^{\mathrm{ADH}}$ and k_6^{ADH}. If not stated differently then the new parameters are chosen equal to the corresponding values of the acetaldehyde reduction, *i.e.* $k_4^{\mathrm{ADH}} = k_1^{\mathrm{ADH}}, k_5^{\mathrm{ADH}} = k_2^{\mathrm{ADH}}$ and $k_6^{\mathrm{ADH}} = k_3^{\mathrm{ADH}}$. The corresponding ODE with gain ($v^+_{\mathrm{ADH,K}}$) and loss ($v^-_{\mathrm{ADH,K}}$) fluxes reads

$$\frac{\mathrm{d}[\mathrm{ADH_K}]}{\mathrm{dt}} = v^+_{\mathrm{ADH,K}} - v^-_{\mathrm{ADH,K}} \tag{8}$$

$$v^+_{\mathrm{ADH,K}} = k_4^{\mathrm{ADH}} \cdot [\mathrm{K}] \cdot [\mathrm{NADH}] \cdot [\mathrm{ADH}] \tag{9}$$

$$v^-_{\mathrm{ADH,K}} = k_5^{\mathrm{ADH}} \cdot [\mathrm{ADH_K}] + k_6^{\mathrm{ADH}} \cdot [\mathrm{ADH_K}] \ . \tag{10}$$

The additional variable $[\mathrm{ADH_K}]$ also alters the constraints and yields via the consumption of [NADH] a strong feedback on the upstream steps of glycolysis.

$$[\mathrm{ADH}] = ADH_{\mathrm{total}} - [\mathrm{ADH_{ACA}}] - [\mathrm{ADH_K}] \tag{11}$$

$$[\mathrm{NAD^+}] = N_{\mathrm{total}} - [\mathrm{NADH}] - [\mathrm{ADH_{ACA}}] - [\mathrm{ADH_K}] \tag{12}$$

The membrane transporters for ketone $v_{\mathrm{K}} = \kappa \cdot ([\mathrm{K}_x] - [\mathrm{K}])$ and carbinol were chosen linear in order not to restrict the accessible range of intracellular perturbations. The permeability for ketone $\kappa = 24.7\ \mathrm{min}^{-1}$ was set equal to the value for acetaldehyde [15].

The above perturbation introduces a competition between acetaldehyde and ketone for unbound enzyme ADH and the cofactor NADH. In Sect. 3, the behavior of both models is tested for consequences of the perturbation and predictions on oscillatory or steady behavior are compared.

2.3 Methods

The investigated metabolic network may be considered as a nonlinear dynamical system that evolves its own state, *i.e.* the set of values for the metabolites' concentrations, in a self-organizing manner. Various computational methods have been developed and proven to be essential for the analysis of complex cellular networks [18,19], *e.g.* bifurcation analysis [20,21] and direct numerical simulation [22].

Since we focus on steady and oscillatory states it is most convenient to combine the computation of the system's state along "branches" in order to efficiently scan the parameter space. This strategy is called "continuation" and starts from a single known solution and proceeds in subsequent steps to compute similar solutions for neighboring values of the parameters, *e.g.* $[\mathrm{Glc}_x]_0$ (mixed flow glucose concentration at inlet), $[\mathrm{K}_x]$ (extracellular ketone concentration). We used the software package AUTO for such tasks [37]. Therein the solutions are represented as the root of an extended system of algebraic equations derived by discretizing the ODEs. Any new solution (the root) is then computed iteratively by the Newton algorithm.

The software also monitors the linear stability of the solutions and thereby detects critical values of the parameters where the solutions change drastically, so called "bifurcations". The onset of oscillations, a Hopf bifurcation, is of special interest here hence the employed strategy amounts to a bifurcation analysis. Bifurcations may themselves be continued in two control parameters simultaneously which was used to fit the parameter set of the core model to flux and concentration data of the full scale model at the Hopf bifurcation. We have supplemented the AUTO package by subroutines for oscillatory states that monitor and export the time averages of fluxes and the relative phase shifts between periodic time courses of concentrations.

3 Results

3.1 Comparison of model predictions

The fluxes within the metabolic network of glycolysis are redirected when the extracellular ketone concentration is increased. Both models show almost identical behavior, see Fig. 3. The effluxes (storage, ethanol, glycerol, acetaldehyde) are represented by the intervals between the curves above and below the corresponding area and all effluxes add up to the total influx in units of C_3. The observed increase in the efflux of acetaldehyde corresponds to the additional

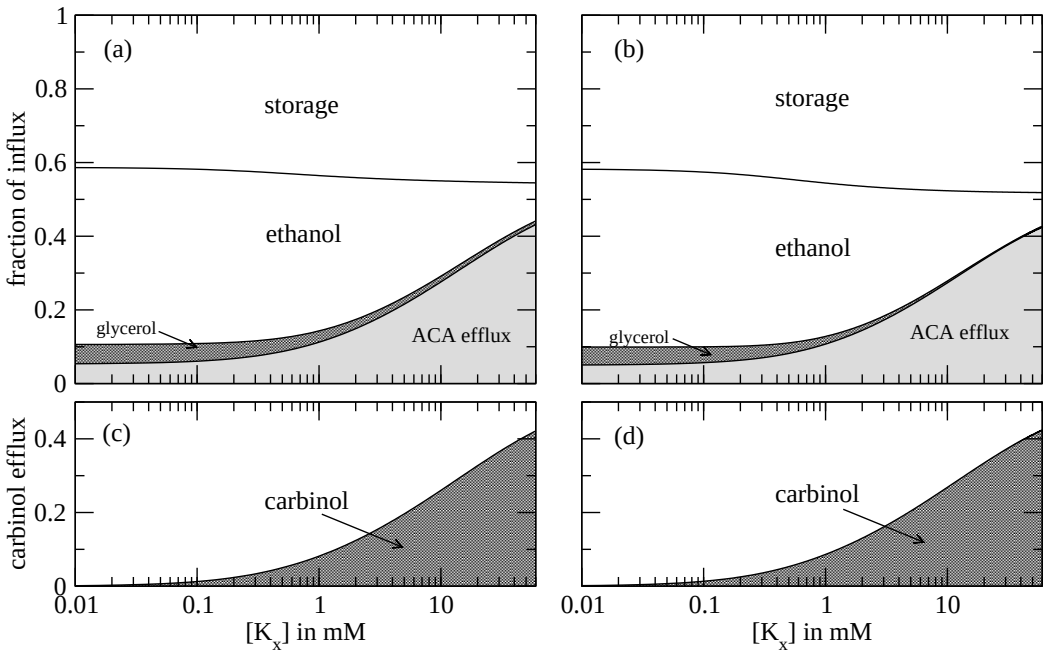

Fig. 3. Flux diagrams (log-linear scales) at fixed glucose concentration $[\mathrm{Glc}_x]_0$=30mM for (a) the full scale model and (b) the core model. All fluxes have been measured in equivalents of C_3 entities and have been normalized by the influx (96.2 mM_{C_3} min^{-1}). Individual pathways (storage, ethanol production, glycerol production, acetaldehyde (ACA) efflux as annotated) consume a portion of the influx given by the distance between the curves above and below the respective area. (c),(d) The biotransformation flux for both models.

consumption of cofactor NADH via ketone reduction. The latter is fostered by increasing ketone concentration, and the stoichiometric constraint on NADH recycling (light shaded area equals sum of dark shaded areas) demands an equal flux of NADH regeneration. Glycerol secretion is discriminated by the lack of NADH, however, in the full scale model a small flux to glycerol remains even for large ketone concentration whereas this flux is strongly suppressed in the core model. We observed the same behavior independently of the value of $[\mathrm{Glc}_x]_0$. Fluxes have been averaged over time for the oscillatory states. Note, the time courses of substrates and cofactors in oscillatory states are generally out of phase which influences the average fluxes, see Subsec. 3.2.

The dependence of the oscillations on the strength of the ketone reduction is shown in Fig. 4. Both models behave differently with sustained oscillations predicted by the full scale model over the whole range of perturbations whereas the core model does favor steady behavior. However, the temporally averaged concentration of NADH shows the same depression upon ketone increase, reflecting the additional NADH consumption.

We repeated the analysis for several values of the carbinol release rate k_6^{ADH} from the ADH complex, see Eq. (7). Different release rates are expected for

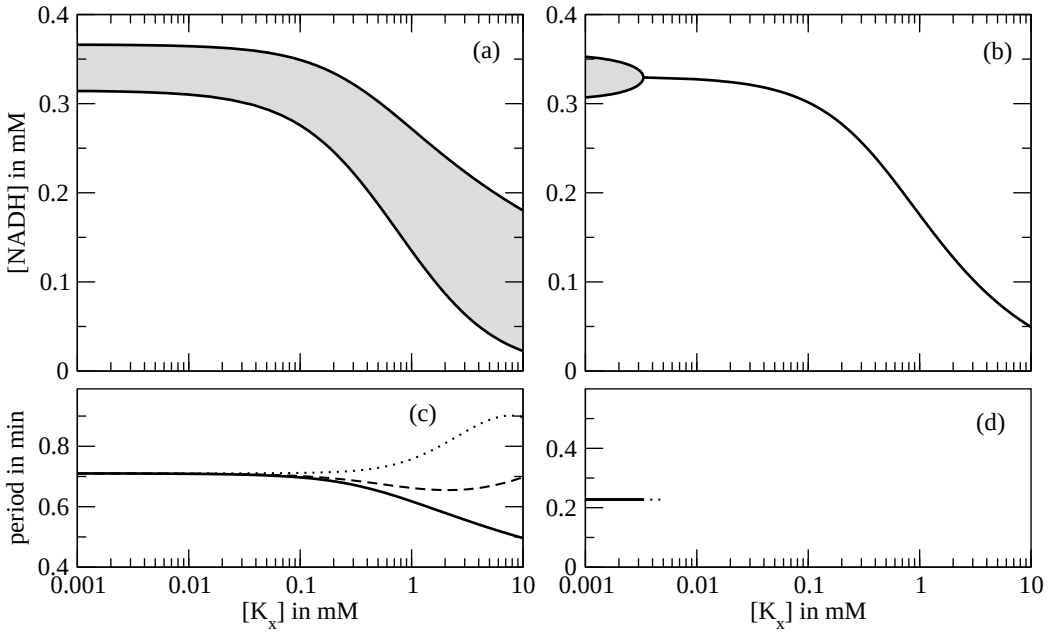

Fig. 4. Bifurcation diagrams for (a),(c) the full scale model and (b),(d) the core model at fixed $[\mathrm{Glc}_x]_0$=30mM. Oscillations of the NADH concentration (gray area in (a),(b)) occur between a maximum and a minimum value (solid curves) that decrease for stronger perturbation by ketone. (c),(d) Temporal period of the oscillations for $k_6^{\mathrm{ADH}} = 5400\ \mathrm{min}^{-1}$ (solid curve) that decreases (frequency increases) with $[\mathrm{K}_x]$ for the full scale model in (c). Additionally, data for $k_6^{\mathrm{ADH}} = 4800\ \mathrm{min}^{-1}$ (dashed) and $k_6^{\mathrm{ADH}} = 3800\ \mathrm{min}^{-1}$ (dotted) indicate that periods may also remain unaffected or increase with $[\mathrm{K}_x]$ depending on the carbinol release rate.

structurally dissimilar ketones due to varying interactions between the enzyme and structures besides the common keto-group. The corresponding variability in the affinity k_4^{ADH} and in k_5^{ADH} are not considered as such changes can be compensated by rescaling of $[\mathrm{K}_x]$ and do not yield new results.

Fig. 4 (c) shows how the oscillation period is affected by ketone for three choices of the release rate k_6^{ADH}. The oscillations speed up (period decreases) for $k_6^{\mathrm{ADH}} > k_{6cr}^{\mathrm{ADH}} = 4800\ \mathrm{min}^{-1}$ including the case of equal release rates $k_3^{\mathrm{ADH}} = k_6^{\mathrm{ADH}}$ and the oscillations slow down (period increases) if the release rate is chosen slower than k_{6cr}^{ADH}. The critical rate k_{6cr}^{ADH} arises from the competition of additional NAD^+ recycling flux due to additional substrate (ketone) versus diminished NAD^+ recycling via ACA reduction when the enzyme is trapped longer in the ADH_K complex and therefore less active. The former effect accelerates the oscillations whereas the latter slows them down. Sustained oscillations have been observed over long time scales [11] which enable accurate measurements of the oscillation period. Such measurements can be used to infer rate constants of different ketones relative to the rates of ACA reduction and to distinguish different ketones.

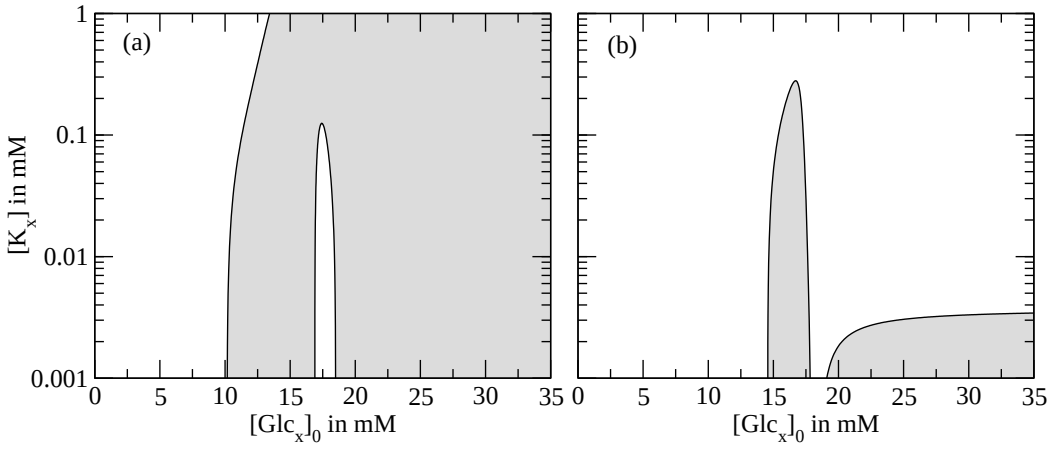

Fig. 5. Phase diagram of stable stationary (white) and oscillatory (gray) states in the $[\mathrm{Glc}_x]_0$ - $[\mathrm{K}_x]$ parameter space (linear-logarithmic scales) for (a) the full scale model and (b) the core model.

Fig. 4 (d) confirms that the core model does not possess the dynamical features discussed above. In order to characterize the conflicting predictions of both models, we have computed the parameter values of the onset of oscillations in a two-parameter plane, see Fig. 5. We observe a qualitative difference in terms of the relations between the three Hopf bifurcations that are present in the unperturbed system. The full scale model possesses extended oscillatory domains (gray shaded). When $[\mathrm{K}_x]$ is increased, two Hopf bifurcations at *large* $[\mathrm{Glc}_x]_0$ are connected and the enclosed steady behavior vanishes. The core model favors stationary states: two Hopf bifurcations at *small* $[\mathrm{Glc}_x]_0$ are connected and the enclosed oscillations vanish when $[\mathrm{K}_x]$ is increased. Hence, the different levels of abstraction mainly determine the dynamical aspects of the models' behavior. On the other hand the averaged or stationary quantities are much less affected by the considered abstraction.

We further examined the case of low membrane permeability for ketone or equivalently low external concentration of ketone (to maintain viability) which both yield small intracellular concentrations of ketone. At a fixed ketone concentration ($[\mathrm{K}_x] < 1$ mM), we varied $[\mathrm{Glc}_x]_0$ and monitored the fluxes. A maximum of carbinol production is found at an intermediate value of $[\mathrm{Glc}_x]_0$ which depends on the fixed value $[\mathrm{K}_x]$ (not shown). Both models predict this maximum which can be interpreted as follows. The lack of NADH recycling is limiting the carbinol flux for small $[\mathrm{Glc}_x]_0$ whereas at large $[\mathrm{Glc}_x]_0$ almost all ADH binds to acetaldehyde which is then much more abundant than the competing ketone. Hence at intermediate value an optimum carbinol flux develops where both limiting influences are weak. In biotechnological applications it is often desired to adjust the glucose supply accordingly.

3.2 Phase shift in oscillatory states

Finally, we have closer analysed possible differences between temporally averaged oscillatory fluxes and the coexisting steady state fluxes, both in the full scale model. Note, the steady states are unstable when oscillations occur supercritically but unstable states can nevertheless be computed by the continuation algorithm as this method does not rely on temporal integration. The unstable steady state represents a solution that equally respects stoichiometric and regulatory constraints as the stable oscillatory state does and a minor change in parameters can render the steady state stable. Hence the coexisting unstable steady state reproduces the behavior of an alternative operational mode.

As an example, we compare the fluxes towards glycerol production for a range of values of the carbinol release rate k_6^{ADH} from the ADH complex, see the remarks above and Eq. (7). Fig. 6 (a) shows a small portion of the reaction scheme of glycolysis where dihydroxyacetone phosphate (DHAP) and NADH are reaction partners. The concentrations of fructose 1,6-bisphosphate (FBP), glyceraldehyde 3-phosphate (GAP) and DHAP perform synchronized oscillations whereas the cofactors NADH and NAD^+ always possess anti-cyclic oscillations. Therefore, this branch point of glycolysis (Fig. 6 (a) and shaded area in Fig. 1 (b)) may act as a switch if the oscillation of either NADH or NAD^+ can be synchronized with the substrate pool.

The computations are performed in the full scale model and all parameters of the glycerol path are kept fixed. Fig. 6 (b) shows the averaged oscillatory glycerol flux that is increased by more than 50% at large rate k_6^{ADH} with respect to the steady state at the same rate. The time courses of substrate DHAP and cofactor NADH are depicted in Fig. 6 (c,d) for two different values of k_6^{ADH}. The temporally averaged concentrations $\langle c \rangle_t$ are almost identical with the steady state value at the same k_6^{ADH}. We define a phase $\phi(c) \equiv 2\pi(t(c_{max}) + t(c_{min}))/2T$ to characterize a time course with period T and time of maximum ($t(c_{max})$) and minimum concentration ($t(c_{min})$). The large increase in averaged oscillatory flux versus the steady state value stems from the oscillations of DHAP and NADH that are almost in phase at large k_6^{ADH} (Fig. 6 (d,e)).

Slower release of NAD^+ (smaller k_6^{ADH}) increases the phase shift ($\Delta\phi \equiv \phi([\mathrm{DHAP}]) - \phi([\mathrm{NADH}])$) to the trailing DHAP oscillation (Fig. 6 (c)) and decreases the averaged oscillatory flux relative to the steady state flux (Fig. 6 (e)). In addition to the phase shift $\Delta\phi$, the averaged oscillatory flux is also affected by changes (due to varied k_6^{ADH}) in amplitude and functional form of the oscillations. Moreover, the absolute values of both steady and averaged oscillatory flux vary strongly (Fig. 6 (b)) as the temporally averaged metabolite

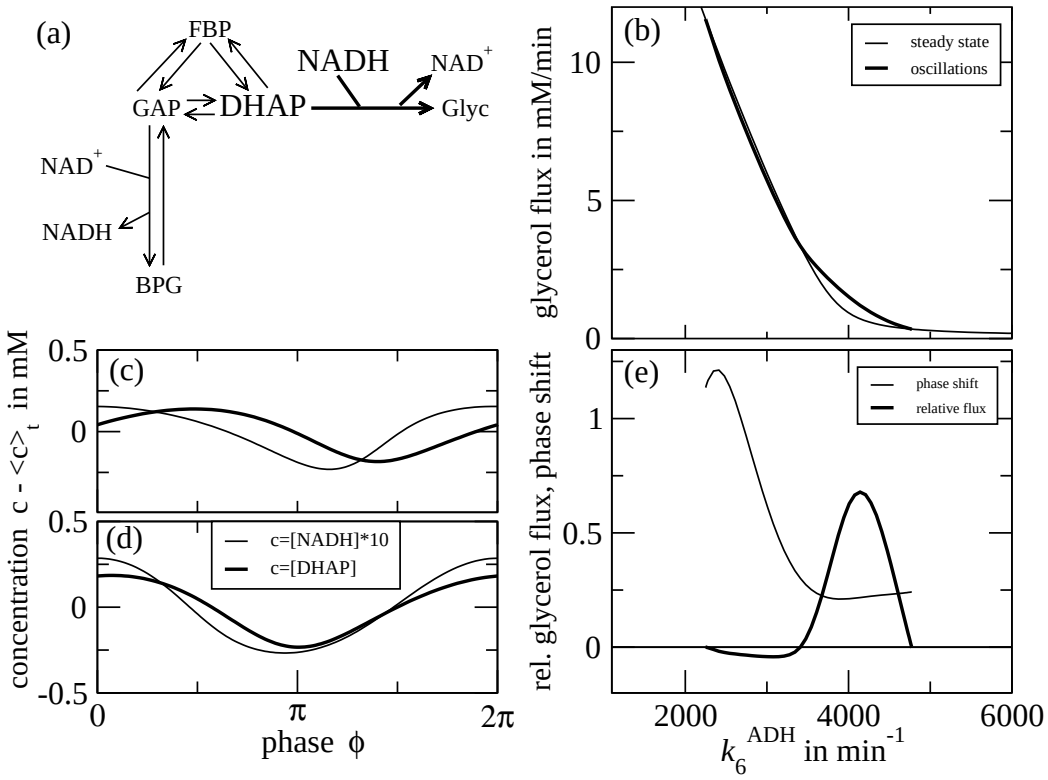

Fig. 6. (a) Small portion of the reaction scheme of glycolysis corresponding to the shaded box in Fig. 1(b). The substrate DHAP is reduced by NADH to finally yield glycerol. (b) Temporally averaged glycerol flux $v_{\rm osc}$ in oscillatory state (thick curve between two Hopf bifurcations at $k_6^{\rm ADH} \approx 2250$ min^{-1} and 4750 min^{-1}) is found to be larger or smaller, respectively, than the corresponding steady state flux $v_{\rm steady}$ (thin curve). (c) Oscillatory time courses of [NADH] (thin) and [DHAP] (thick curve) are out of phase by $\Delta\phi = 1.2$ at $k_6^{\rm ADH}$=2300 min^{-1}. Average concentrations $\langle c\rangle_t$ have been subtracted and [NADH] has been scaled by a factor of 10 in (b,c). (d) Both concentrations oscillate almost in phase ($\Delta\phi = 0.2$) at larger $k_6^{\rm ADH}$, here 4600 min^{-1}. (e) The relative difference of fluxes $(v_{\rm osc} - v_{\rm steady})/v_{\rm steady}$ (thick) is partly due to varying phase shift $\Delta\phi$ (thin curve) between the time courses of substrate DHAP and cofactor NADH. Parameters are $[{\rm Glc}_x]_0$=15mM and $[{\rm K}_x]$=10mM.

concentrations change with $k_6^{\rm ADH}$. The biotransformation flux towards carbinol is affected by changes of similar absolute size which, however, amount to slight relative changes only.

In the left half of the oscillatory interval, the averaged oscillatory flux to glycerol is even smaller than in steady state which is only possible for a large phase shift, as observed in Fig. 6 (c). The effect of the phase shift becomes dominant for large oscillation amplitudes because it clearly matters, if the reaction partners frequently collide when they appear at the same time or if they only rarely react when one of them is always too late. This situation is analogous to a problem in electrical engineering where the electrical power at a device in a sinusoidal alternating current (AC) depends on the amplitudes

of voltage and current and on the phase shift between their maxima.

4 Conclusions and perspective

We have compared predictions of two theoretical models that have previously been used to describe glycolytic oscillations in yeast. Both models possess the same topology but incorporate different levels of kinetic details. Irrespective of these differences, both models predicted identical dependencies of temporally averaged fluxes and concentrations on the strength of the perturbation, *i.e.* the extracellular concentration of a xenobiotic ketone. This observation provides confidence in theoretical modeling given the topology of the network is known and completely incorporated. Note, the unknown parameters of the models were fitted to data of the unperturbed system hence the models predicted the response to the perturbation. The chosen perturbation affected the entire network via multiple feedback loops of cofactors. We suggest the exposure to xenobiotics as a feasible experimental probe of the network's global response. In the future we will extend this analysis to metabolic responses in other eucaryotes and to a range of pharmacologically active compounds.

The kinetic details of both models affected the temporal organisation of the responses. Oscillations ceased to exist in the abstract core model while the full scale model supported oscillations for a large range of perturbations. Oscillatory behavior has recently been suggested by Hauser *et al.* to protect enzymes and possibly cells against toxic substances [38,39]. Oscillations also play an important role for calcium signal transduction [40] where they appear in bursts [41,42]. Bursting, the temporally repeated sequence of quiescent and oscillating episodes, has recently been found in a theoretical study of stochastically driven glycolysis [43]. Oscillations have also been suggested to improve the thermodynamic efficiency of glycolysis with respect to steady operation [44]. Furthermore, kinetic details are important for (non periodic) short term responses to glucose pulses [10].

A closer inspection of the flux distribution in oscillatory states revealed that temporally averaged fluxes may differ from the values in the coexisting (unstable) steady state, albeit for each metabolite the (unstable) steady state concentration equals the temporally averaged value in the oscillatory state. This effect results from the relative phase shift between time courses of substrates and cofactors particularly at branch points of the network. The time average of any oscillatory flux is generally restricted to a convex combination of elementary flux modes [45]. However, allosterically regulated enzymes impose additional restrictions on the fluxes at given metabolite concentrations which can result in suboptimal convex combinations particularly in steady states. Oscillatory states possess additional degrees of freedom, *i.e.* phase shifts, that

are adjusted by many even remote reactions. Evolution of metabolic networks may therefore have acted faster on those networks capable of oscillatory behavior enabling them to explore more possibilities and to become superior. This conjecture is in line with the observed oscillatory behavior in one of the most important and inherited metabolic pathways, *i.e.* glycolysis, and it supports the view that oscillatory behavior may be more abundant than presently recognised [38,39].

A corresponding strategy for metabolic engineering may target the phase shifts in oscillatory states as has been suggested by Ross and coworkers [46]. They forced simple reaction schemes with oscillating substrate concentrations to increase desired fluxes. Here we found that the same effect is also important for large metabolic networks where phase shifts are adjusted in a self-organizing fashion. The artificial addition of appropriate buffers or bypasses (as in the present example) in order to control phase shifts are promising candidates for metabolic engineering.

In terms of modeling strategies, one should treat those approaches with caution that focus on steady states, *e.g.* canonical modeling [47], since the computed flux distribution in an unstable steady state does not necessarily approximate the actual oscillatory behavior around that steady state. Continuation algorithms as applied in the present paper appear to be particularly suited to address the (dis)advantages of oscillatory versus (hypothetical) stationary behavior.

To summarize, we have shown that static features of the metabolic network of glycolysis are robust to crude abstractions of models but more care has to be taken when dynamic features are considered. Many open questions remain and call for further research work. E.g. the possibility to conduct ketone-to-carbinol biotransformations under aerobic conditions could increase the NADH recycling and hence the carbinol production which, *per se*, is an important biotechnological challenge. Further modeling will help to solve the related problems by simulating the effect of suppressing or enhancing parts of the complex metabolic network.

We are indebted to Markus Bär, Sune Danø, Jean-Marie François, Ursula Kummer, Karl-Heinz van Pée, Preben Graae Sørensen and Jana Wolf for fruitful discussions. MB wishes to thank Gerhard Jörg for practical assistance and the Graduate Research Center "Heterocycles" as well as the German National Merit Foundation for financial support.

References

[1] S. G. Oliver, *From DNA sequence to biological function*, Nature **379**, 597 (1996).

[2] G. L. G. Miklos and G. M. Rubin, *The role of the genome project in determining gene function: Insights from model organisms*, Cell **86**, 521 (1996).

[3] T. I. Lee, *Transcriptional regulatory networks in Saccharomyces cerevisiæ*, Science **298**, 799 (2002).

[4] *Biochemical pathways: An atlas of biochemistry and molecular biology*, edited by G. Michal (John Wiley & Sons, Inc., New York, 1998), p. 277.

[5] J. von Dassow, E. Meir, E. M. Munro, and G. M. Odell, *The segment polarity network is a robust developmental module*, Nature **406**, 188 (2000).

[6] C. C. Guet, M. B. Elowitz, W. Hsing, and S. Leibler, *Combinatorial synthesis of genetic networks*, Science **296**, 1466 (2002).

[7] H. V. Westerhoff *et al.*, *General discussion*, Faraday Discuss. **120**, 325 (2001).

[8] S. Ostergaard, L. Olsson, and J. Nielsen, *Metabolic engineering of Saccharomyces cerevisiæ*, Microbiol. Mol. Biol. Rev. **64**, 34 (2000).

[9] B. Sonnleitner, *Yeast - a model system in biotechnology*, Swiss Pharma **18**, 10 (1996).

[10] M. Rizzi, M. Baltes, U. Theobald, and M. Reuss, *In vivo analysis of metabolic dynamics in Saccharomyces cerevisiæ: II. Mathematical model*, Biotech. and Bioeng. **55**, 592 (1997).

[11] S. Danø, P. G. Sørensen, and F. Hynne, *Sustained oscillations in living cells*, Nature **402**, 320 (1999).

[12] J. Wolf and R. Heinrich, *Effect of cellular interaction on glycolytic oscillations*, Biochem. J. **345**, 321 (2000). The Silicon Cell version of a related model is online at `http://www.jjj.bio.vu.nl/database/wolf`

[13] J. Wolf, J. Passarge, O. J. G. Somsen, J. L. Snoep, R. Heinrich, and H. V. Westerhoff, *Transduction of intracellular and intercellular dynamics in yeast glycolytic oscillations*, Biophys. J. **78**, 1145 (2000).

[14] B. Teusink *et al.*, *Can yeast glycolysis by understood in terms of in vitro kinetics of the constituent enzymes? Testing biochemistry.*, Eur. J. Biochem. **267**, 5313 (2000).

[15] F. Hynne, S. Danø, and P. G. Sørensen, *Full-scale model of glycolysis in Saccharomyces cerevisiæ*, Biophys. Chem. **94**, 121 (2001). The Silicon Cell version of this model is online at `http://www.jjj.bio.vu.nl/database/hynne`

[16] K. A. Reijenga, H. V. Westerhoff, B. N. Kholodenko, and J. L. Snoep, *Control analysis for autonomously oscillating biochemical networks*, Biophys. J. **82**, 99 (2002).

[17] R. Heinrich and S. Schuster, *The regulation of cellular systems* (Kluwer Academic Publishers, Boston, 1996), p. 372.

[18] J. J. Tyson, K. Chen and B. Novak, *Network dynamics and cell physiology*, Nature Rev. Mol. Cell Biol. **2**, 908 (2001).

[19] C. P. Fall, E. Marland, J. M. Wagner and J. J. Tyson, *Computational cell biology*, (Springer, New York, 2002).

[20] S. H. Strogatz, *Nonlinear dynamics and chaos*, (Addison-Wesley Co., Reading, Massachusetts, 1994).

[21] D. Kaplan and L. Glass, *Understanding nonlinear dynamics*, (Springer, New York, 1995).

[22] P. Mendes, *Biochemistry by numbers: simulation of biochemical pathways with Gepasi 3*, Trends in Biochemical Sciences **22**, 361 (1997).

[23] L. Calabrese and A. B. Fleischer, *Thalidomide: current and potential clinical applications*, Am. J. Med. **108**, 487 (2000).

[24] M. Bertau, M. Bürli, P. Wagner, and E. Hungerbühler, *A novel highly stereoselective synthesis of chiral 5- and 4,5-substituted 2-oxazolidinones*, Tetrahedron: Asymmetry **12**, 2303 (2001).

[25] P. Davoli, A. Forni, I. Moretti, F. Prati, G. Torre, *D-(1) and L-(2) ethyl 4,4,4- trifluoro-3-hydroxy butanoate by enantioselective baker's yeast reduction*, Enzyme Microb. Technol. **25**, 149 (1999).

[26] O. Cabon, D. Buisson, M. Larcheveque, R. Azerad, *The microbial reduction of 2-chloro-3-oxoesters*, Tetrahedron: Asymmetry **6**, 2199 (1995).

[27] M. Bertau, *Novel unusual microbial dehalogenation during enantioselective reduction of ethyl 4,4,4-trifluoro acetoacetate with bakers yeast*, Tetrahedron Lett. **42**, 1267 (2001).

[28] M. Bertau, *How cell physiology affects enantioselectivity of the biotransformation of ethyl 4-chloro-acetoacetate with Saccharomyces cerevisiæ*, Biocatal. Biotransform. **20**, 363 (2002).

[29] J. François, and J. L. Parrou, *Reserve carbohydrates metabolism in the yeast Saccharomyces cerevisiæ*, FEMS Microbiol. Rev. **25**, 125 (2001).

[30] F. Beaudoin, K. Gable, O. Sayanova, T. Dunn, J. A. Napier, *A Saccharomyces cerevisiæ gene required for heterologous fatty acid elongase activity encodes a microsomal beta-keto-reductase*, J. Biol. Chem. **277**, 11481 (2002).

[31] E. Gonzalez, M. R. Fernandez, C. Larroy, L. Sola, M. A. Pericas, X. Pares, J. A. Biosca, *Characterization of a (2R,3R)-2,3-butanediol dehydrogenase as the Saccharomyces cerevisiæ YAL060W gene product. Disruption and induction of the gene*, J. Biol. Chem. **275**, 35876 (2000).

[32] A. C. Dahl, J.O. Madsen, *Bakers yeast: production of D- and L-3-hydroxy esters*, Tetrahedron: Asymmetry **9**, 4395 (1998).

[33] M. North, *Bakers yeast reduction of β-keto esters in petrol*, Tetrahedron Lett. **37**, 1699 (1996).

[34] N. Mochizuki, T. Sugai, H. Ohta, *Biochemical reduction of 3-oxoalkanoic esters by a bottom-fermentation yeast, Saccharomyces cerevisiæ IFO 0565*, Biosci. Biotech. Biochem. **58**, 1666 (1994).

[35] T. Kometani, E. Kitatsuji, R. Matsuno, *Bioreduction of ketones mediated by bakers yeast with acetate as ultimate reducing agent*, Agric. Biol. Chem. **55**, 867 (1991).

[36] W. F. H. Sybesma, A. J. J. Straathof, J. A. Jongejan, J. T. Pronk, J. J. Heijnen, *Reductions of 3-oxo esters by bakers yeast: current status*, Biocatal. Biotransform. **16**, 95 (1998).

[37] E. Doedel *et al.*, *AUTO97: Continuation and bifurcation software for ordinary differential equations*, (Concordia University, Montreal, 1997).

[38] M. J. B. Hauser, U. Kummer, A. Z. Larsen and L. F. Olsen, *Oscillatory dynamics protect enzymes and possibly cells against toxic substances*, Faraday Discuss. **120**, 215 (2001).

[39] L. F. Olsen, M. J. B. Hauser, U. Kummer, *Mechanism of protection of peroxidase activity by oscillatory dynamics*, Eur. J. Biochem. **270**, 2796 (2003).

[40] M. J. Berridge, M. D. Bootman and P. Lipp, *Calcium - a life and death signal*, Nature **395**, 645 (1998).

[41] U. Kummer, L. F. Olsen, C. J. Dixon, A. K. Green, E. Bornberg-Bauer and G. Baier, *Switching from simple to complex oscillations in calcium signaling*, Biophys. J. **79**, 1188 (2000).

[42] L. Brusch, W. Lorenz, M. Or-Guil, M. Bär and U. Kummer, *FoldHopf bursting in a model for calcium signal transduction*, Z. Phys. Chem. **216**, 487 (2002).

[43] S. Kar and D. S. Ray, *Collapse and revival of glycolytic oscillation*, Phys. Rev. Lett. **90**, 238102 (2003).

[44] P. H. Richter and J. Ross, *Oscillations and efficiency in glycolysis*, Biophys. Chem. **12**, 285 (1980).

[45] S. Schuster, T. Dandekar and D. A. Fell, *Detection of elementary flux modes in biochemical networks: a promising tool for pathway analysis and metabolic engineering*, Trends Biotechnol. **17**, 53 (1999).

[46] J. G. Lazar and J. Ross, *Changes in mean concentration, phase shifts, and dissipation in a forced oscillatory reaction*, Science **247**, 189 (1990).

[47] E. O. Voit, *Computational analysis of biochemical systems. A practical guide for biochemists and molecular biologists*, (Cambridge University Press, Cambridge, 2000).